Available online at www.sciencedirect.com
SCIENCE DIRECT®
ELSEVIER
Journal of Nuclear Materials 320 (2003) 231–244
journal of nuclear materials
www.elsevier.com/locate/jnucmat

Enthalpies of formation of U-, Th-, Ce-brannerite: implications for plutonium immobilization

K.B. Helean [a,*], A. Navrotsky [a], G.R. Lumpkin [b], M. Colella [b], J. Lian [c], R.C. Ewing [c], B. Ebbinghaus [d], J.G. Catalano [e]

[a] *Thermochemistry Facility, Department of Chemical Engineering and Materials Science, The University of California at Davis, Davis, CA 95616, USA*

[b] *Australian Nuclear Science Technology Organization, Private Mailbag 1, Menai (Sydney), NSW 2234, Australia*

[c] *Department of Nuclear Engineering & Radiological Sciences and Materials Science & Engineering, University of Michigan, Ann Arbor, MI 48109-2104, USA*

[d] *Lawrence Livermore National Laboratory, P.O. Box 808, Livermore, CA 94551, USA*

[e] *Department of Geological and Environmental Sciences, Stanford University, Palo Alto, CA 94305, USA*

Received 17 June 2002; accepted 24 February 2003

Abstract

Brannerite, ideally MTi_2O_6, (M = actinides, lanthanides and Ca) occurs in titanate-based ceramics proposed for the immobilization of plutonium. Standard enthalpies of formation, ΔH_f^0 at 298 K, for three brannerite compositions (kJ/mol): $CeTi_2O_6$ (-2948.8 ± 4.3), $U_{0.97}Ti_{2.03}O_6$ (-2977.9 ± 3.5) and $ThTi_2O_6$ (-3096.5 ± 4.3) were determined by high temperature oxide melt drop solution calorimetry at 975 K using $3Na_2O \cdot 4MoO_3$ solvent. The enthalpies of formation were also calculated from an oxide phase assemblage ($\Delta H_{f\text{-}ox}^0$ at 298 K): $MO_2 + 2TiO_2 = MTi_2O_6$. Only UTi_2O_6 is energetically stable with respect to an oxide assemblage: $U_{0.97}Ti_{2.03}O_6$ ($\Delta H_{f\text{-}ox}^0 = -7.7 \pm 2.8$ kJ/mol). Both $CeTi_2O_6$ and $ThTi_2O_6$ are higher in enthalpy with respect to their oxide assemblages with ($\Delta H_{f\text{-}ox}^0 = +29.4 \pm 3.6$ kJ/mol) and ($\Delta H_{f\text{-}ox}^0 = +19.4 \pm 1.6$ kJ/mol) respectively. Thus, Ce- and Th-brannerite are entropy stabilized and are thermodynamically stable only at high temperature.

PACS: 65.50.+m; 61.16.Bg; 61.66.–f

1. Introduction

Brannerite, nominally $M_xTi_{3-x}O_6$, where $0.7 < x < 1.1$ and M = U, Th, Ce, Ca, is a common accessory phase found in uranium ore deposits and is one of the principal uranium ore minerals [1–3]. Synthetic brannerite also occurs as a minor phase in the actinide-rich formulations of Synroc, a titanate ceramic proposed for the immobilization of high level radioactive waste [4]. In some formulations brannerite comprises up to 30 wt% of a pyrochlore-based ceramic waste form proposed for Pu immobilization [5–7]. Despite the importance of brannerite as an actinide-host in titanate waste forms, the thermodynamic data for this phase have previously been poorly constrained [3]. Brannerite is susceptible to radiation-induced amorphization from alpha-decay of actinides, and damage accumulation models require a knowledge of relevant thermodynamic parameters as a function of composition [8,9].

The structure of brannerite (C2/m) consists of sheets of edge-sharing TiO_6-octahedra parallel to the *b*-axis (Fig. 1, top) [1]. The TiO_6-octahedral sheets are distorted so as to resemble the structure of anatase, TiO_2, with the TiO_6 polyhedra connected by columns of

* Corresponding author. Tel.: +1-530 754 2132; fax: +1-530 752 9703.
E-mail address: kbhelean@ucdavis.edu (K.B. Helean).

0022-3115/03/$ - see front matter © 2003 Elsevier B.V. All rights reserved.
doi:10.1016/S0022-3115(03)00186-7

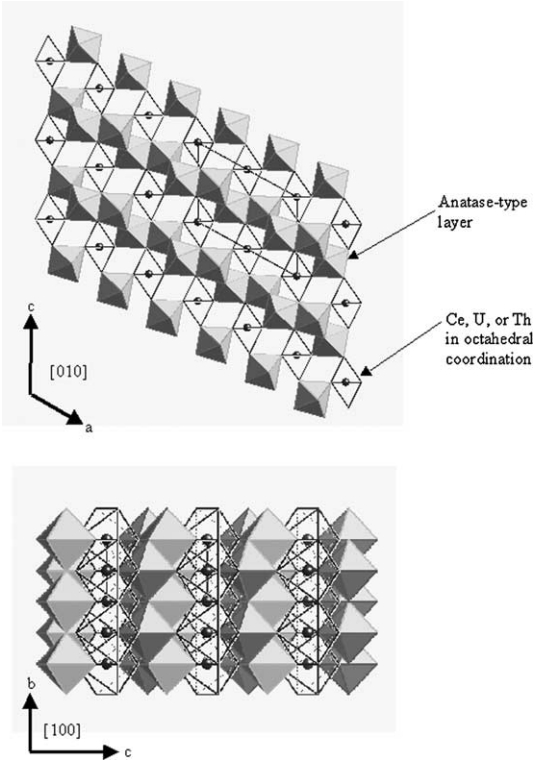

Fig. 1. The crystal structure of brannerite. TiO_6-octahedra share edges to form a zig-zag layer similar to the anatase structure. The large A-site cations (Ce, U, or Th) occupy octahedral sites in the interlayer.

UO_6-octahedra (Fig. 1, bottom). The UO_6-octahedra are nearly regular in shape and share edges much like the octahedra in rutile [11]. Each Ti-octahedron shares three edges with other Ti-octahedra and three corners with U-octahedra. Ce and Th can substitute onto the U-site with little additional distortion of the octahedra [1].

Cerium is commonly used to estimate the properties of solids containing plutonium owing to their similar ionic radii (Ce(IV) = 0.087 nm; Pu(IV) = 0.086 nm for CN = 6) [10]. The compound $CeTi_2O_6$ is isostructural with $PuTi_2O_6$ [12,13]. In this study a calorimetric investigation of $CeTi_2O_6$ was undertaken in order to estimate the thermodynamic properties of $PuTi_2O_6$.

Natural brannerite samples typically contain a number of cations in solid solution on both the U- and Ti-sites [3,8,14,15]. Typical compositions consist of Pb, Ca, Th, Y, Ce on the U-site and Si, Al, Fe on the Ti-site [1,15,19]. Invariably, natural brannerite is metamict (aperiodic) due to radiation damage caused by alpha-decay events of the constituent U, Th and radionuclides in their decay chains [1,20,21]. Radiation damage in waste form phases generally causes swelling, resulting in microfracturing that in turn reduces the chemical durability of natural brannerite by the increased leachability of the aperiodic material and by increasing the total leachable surface area [8,9].

The uranium in natural brannerite is almost always partially oxidized [3]. With complete oxidation, i.e., U(IV) to U(VI), brannerite decomposes to $UTiO_5$ and TiO_2 according to the reaction: $2UTi_2O_6 + O_2 \rightarrow 2UTiO_5 + 2TiO_2$ [16,17]. $UTiO_5$ has been reported to be sub-stoichiometric, containing some U(V) [18]. This suggests that natural brannerite may contain U(V) as well as U(VI). A recent study reported that when aliovalent cations substitute for uranium in synthetic brannerite, charge balance is maintained by the oxidation of U(IV) to U(V) [11]. An absorption band at 1448 nm, using diffuse reflectance spectroscopy, was observed in Ca- and Gd-doped U-brannerite that was attributed to an electronic transition in U(V) [11]. Therefore, aliovalent uranium is possible in synthetic brannerite samples with charge compensation provided by impurity cations. X-ray absorption near edge structure (XANES) was used to determine the oxidation state of U in the brannerite sample in this study.

The purpose of this study is to experimentally determine the enthalpies of formation of three brannerite compositions: $CeTi_2O_6$, UTi_2O_6 and $ThTi_2O_6$. Because they are refractory, high temperature oxide melt solution calorimetry was used to measure the heats of solution for the compounds and their binary oxides. These data were used to estimate the enthalpy of formation of $PuTi_2O_6$ and to assess the impact on waste form stability due to the presence of large amounts (up to 30 wt%) of brannerite [6,7].

2. Sample synthesis

The Ce-brannerite starting material was prepared by ball-milling stoichiometric portions of the oxides, CeO_2 and TiO_2, anatase. The mixture was pressed into a pellet and sintered in air at 1350 °C for >100 h. The U-brannerite sample was synthesized by sintering the oxides, UO_2 and TiO_2, anatase for 300 h in an atmosphere of 5% CO/95% CO_2 at 1200 °C. The initial mixture was slightly enriched in Ti as this was necessary to achieve a single phase sample, possibly because the initial anatase contained some water. The Th-brannerite sample was synthesized by sintering stoichiometric portions of the oxides, ThO_2 and TiO_2, anatase. The mixture was pressed into a pellet and sintered in air at 1500 °C for >100 h. Synthesis results were confirmed by powder X-ray diffraction analysis.

3. Analytical methods

3.1. X-ray powder diffraction

X-ray powder diffraction (XRD) was conducted using a Scintag PAD-V diffractometer with a Cu-anode

and an accelerating voltage of 45 kV over an angular range, $2\theta = 15$–$90°$ and 0.02° step size with a dwell time of 7 s. Rietveld analysis of the XRD data was completed using both the general structure analysis system (GSAS) and the RIQAS system [19,22].

3.2. Electron microprobe analysis

Quantitative chemical analysis was obtained using a Cameca SX50 electron microprobe (EMPA) with wavelength dispersive spectroscopy (WDS), an accelerating voltage of 20 kV, a probe current of 10 nA and a spot size of 1 μm. The following analytical standards were used: U-metal, thoria (ThO_2), cerianite (CeO_2) and rutile (TiO_2).

3.3. X-ray absorption near edge structure spectroscopic analysis

In order to evaluate the oxidation state of U in U-brannerite, shifts in the U L_{III}-edge were measured using XANES spectroscopic analysis. XANES measurements were completed at the Stanford Synchrotron Radiation Laboratory (SSRL) on wiggler beamline 4-3 using a Si(2 2 0) monochrometer in the $\phi = 0°$ orientation. Data were collected in transmission mode at room temperature with the sample perpendicular to the beam. Energy was calibrated using a Y-metal foil; the first inflection points of the Y K-absorption edge was set at 17 038 eV. Data were processed using EXAFSPAK [23]. The following analytical standards were used: $UO_{2.08}$ (a U(IV) standard) and γ-UO_3 (a U(VI) standard).

3.4. High-resolution transmission electron microscopy

High-resolution transmission electron microscopy (HRTEM) was used to assess the crystallinity of the synthesized brannerite samples. A JEOL 2010F electron microscope with a field emission source at the University of Michigan was used at an accelerating voltage of 200 kV. Both bright-field and high-resolution imaging were used to characterize the nanoscale-structure of the samples. Samples were prepared by polishing to thin, electron-transparent wedges using an Ar-ion mill.

3.5. Electron energy loss spectroscopy

Electron energy loss spectroscopy (EELS) was performed using a JEOL 2010F equipped with a Gatan Imaging Filter (GIF) at the Australian Nuclear Science and Technology Organization. Using an operating voltage of 197 kV, spectra were collected for the Ce $M_{IV,V}$, U $M_{IV,V}$ and Ti $L_{II,III}$ edges in Ce-brannerite and U-brannerite. For comparison, additional spectra were obtained from reference samples, including TiO_2, Ti_2O_3, CeO_2, $CePO_4$, UO_2 and $CaUO_4$. Data were acquired in image diffraction mode using pixel dispersions of 0.1–1.0 eV, depending on the element. The spectra for Ti also include the O K edge at 532 eV, which is used as an internal calibration of the energy scale. Based on measurements of the full width at half maximum of the zero loss peak, the energy resolution is approximately 1.0 eV.

4. Sample descriptions

4.1. Ce-brannerite: $CeTi_2O_6$

The refined lattice parameters for the Ce-brannerite sample are similar to those reported for stoichiometric UTi_2O_6 (Table 1) [1]. There is a slight (0.003 nm, 0.2%) increase in the *a*-parameter and a corresponding decrease in *c* (0.002 nm, 0.5%). This indicates a slight distortion of the octahedral M-site in order to accommodate the smaller Ce-ion. The refined lattice parameters suggest that, within the anatase-type TiO_6 layer, a lengthening of bonds occurs in the *a*-direction. This is apparently necessary to compensate for the reduction of the *c*-parameter that results in bringing the anatase-type layers closer together.

One impurity phase, CeO_2, was identified by XRD. Quantitative phase analysis using the Rietveld method indicated that the Ce-brannerite sample consisted of 0.976(2) weight fraction $CeTi_2O_6$ and 0.024(2) weight fraction CeO_2 (Table 1). Converting to mole percent the sample consisted of 95.5 mol% $CeTi_2O_6$ and 4.5 mol% CeO_2.

The CeO_2 impurity was also observed in back-scattered electron (BSE) images (Fig. 2). Semi-quantitative analysis of digital images indicated that the Ce-brannerite sample consisted of 2.5 vol.% CeO_2 and 97.5 vol.% $CeTi_2O_6$. Using the calculated densities for CeO_2 (7.194 g/cm^3) and $CeTi_2O_6$ (4.966 g/cm^3) the estimated volume percents were converted to weight percent: 3.6% CeO_2 and 96.4% $CeTi_2O_6$. This is in reasonable agreement with the results from powder XRD.

The sample was analyzed using EMPA-WDS against the following standards, CeO_2, cerianite and TiO_2, rutile. Oxygen was estimated on the basis of stoichiometry (Table 2). The measured Ce and Ti contents are, within error, equal to the expected stoichiometric values. The Ce-brannerite is therefore, $CeTi_2O_6$.

The EELS data (Fig. 3(a) and (b)) demonstrate that both Ti and Ce are predominantly tetravalent. Fig. 3(a) shows that the main peak positions of Ti in Ce-brannerite (460.0, 462.1, 465.4, 467.5 eV) are nearly identical to those of Ti in the TiO_2 reference sample (459.7, 461.8, 465.1, 467.2 eV) and only minor differences in the peak amplitudes were observed. For comparison, the main $L_{II,III}$ peak positions for Ti in the trivalent reference sample (Ti_2O_3) are shifted by about

Table 1
Lattice parameters and quantitative phase analysis for the three brannerite samples determined by Rietveld refinement of powder XRD data

Phases	Brannerite lattice parameters (nm)				Weight frxn
	a	*b*	*c*	*β*	
$CeTi_2O_6$	0.98305(5)	0.37536(1)	0.68919(2)	119.203(2)	0.976(2)
CeO_2					0.024(2)
$ThTi_2O_6$	0.98046(8)	0.38187(3)	0.70229(5)	118.852(5)	0.991(3)
ThO_2					0.009(1)
UTi_2O_6	0.98043(5)	0.37632(2)	0.69152(3)	118.894(4)	0.982(10)
UO_2					0.004(0)
TiO_2					0.014(1)
Reference data[a]					
UTi_2O_6	0.98123(15)	0.37697(6)	0.69253(9)	118.957(6)	

Lattice parameters are reported in nm with the error on the last digit in parentheses.
[a] Ref. [1].

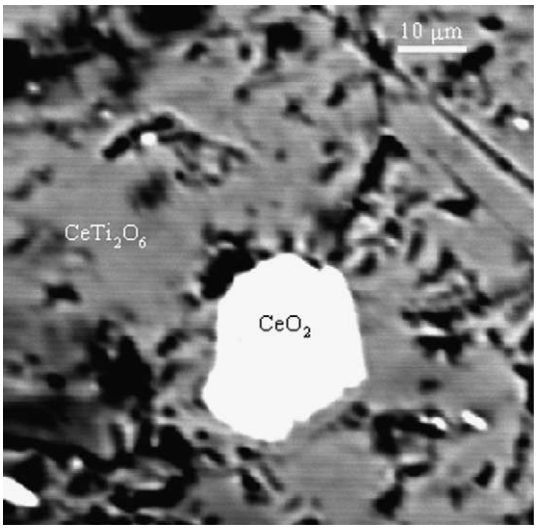

Fig. 2. BSE micrograph of the Ce-brannerite sample showing the presence of cerianite impurity (bright areas) in the Ce-brannerite matrix (gray). The black areas are pore spaces.

−2 eV and the two weaker $L_{II,III}$ peaks on the low energy side (due to molecular orbital splitting) are poorly resolved.

Because the O K edge intensity cannot be collected in the vicinity of the Ce $M_{IV,V}$ edge, the spectra for Ce are aligned on the Ce M_{IV} edge. Results for Ce are shown in Fig. 3(b) and reveal that the main peak amplitudes are nearly identical for Ce-brannerite and the CeO_2 standard. The Ce M_{IV}/M_V ratios for the sample and reference material are both approximately 1.1. For comparison, the Ce M_{IV}/M_V ratio is 0.8 in the trivalent Ce reference material $CePO_4$. The energy loss fine structure is similar in both samples, except for the presence of a distinct peak at approximately 920 eV in the spectrum of the CeO_2 standard. This feature is probably due to differences in the local coordination environment around Ce in the two structure types.

The CeO_2 impurity was not observed in bright field TEM images (Fig. 4, top). HRTEM micrographs and selected area electron diffraction (SAED) indicated that the $CeTi_2O_6$ phase was crystalline with no apparent structural defects observed on the nanoscale (Fig. 4, bottom).

4.2. U-brannerite: UTi_2O_6

The refined lattice parameters for the U-brannerite sample are slightly less (0.001 nm) than those previously reported for stoichiometric UTi_2O_6 (Table 1) [1]. This is consistent with the U-deficiency observed in the sample (see below). Two impurity phases, UO_2 and TiO_2, rutile, were identified by XRD. Quantitative phase analysis using the Rietveld method indicated that the U-brannerite sample consisted of 0.982(10) weight fraction U-brannerite, 0.004(0) weight fraction UO_2 and 0.014(1) TiO_2 (Table 1). This converts to 92.5 mol% U-brannerite, 0.6 mol% UO_2 and 6.9 mol% TiO_2.

The UO_2 impurity was also observed in BSE images. The rutile impurity that was observed in the XRD pattern was not observed by BSE. This could be due to the presence of fine-grained TiO_2 too small to be detected by the microprobe. Therefore, digital image analysis was not used to estimate the impurity content of this sample.

The U-brannerite sample was analyzed using EMPA-WDS against U metal and TiO_2, rutile, standards. Oxygen was estimated on the basis of stoichiometry (Table 2).

Table 2
Results of EMPA-WDS analysis for Ce-brannerite, U-brannerite and Th-brannerite

	Measured data		Nominal values: $CeTi_2O_6$	
	Ave(12)	Error		
Ce-brannerite				
O	28.76	0.19	O	28.93
Ce	42.44	0.34	Ce	42.22
Ti	28.53	0.25	Ti	28.85
Total	99.73	0.60	Total	100.00
	Ave(6)	Error	Nominal values: UTi_2O_6	
U-brannerite				
O	21.95	0.15	O	22.34
U	52.68	0.50	U	55.38
Ti	22.25	0.20	Ti	22.34
Total	96.88	0.65	Total	100.00
	Ave(12)	Error	Nominal values: $ThTi_2O_6$	
Th-brannerite				
O	22.45	0.34	O	22.65
Th	54.72	0.98	Th	54.75
Ti	22.31	0.33	Ti	22.60
Total	99.48	1.59	Total	100.00

Data are reported as weight percent element. Averages of measured data are reported. Nominal values are reported for comparison. Errors are 2σ.

The measured U content was lower by two percent than the stoichiometric value. The Ti was correspondingly high. This is consistent with observations that natural U-brannerite is commonly uranium deficient and Ti-rich [13]. The calculated stoichiometry of the U-brannerite was $U_{0.97}Ti_{2.03}O_{6.00}$.

The XANES spectrum of U-brannerite was compared to $UO_{2.08}$ (a U(IV) standard) and to γ-UO_3 (a U(VI) standard) to evaluate the oxidation state of U in the sample (Fig. 5). The $UO_{2.08}$ and the γ-UO_3 spectra are consistent with published spectra of UO_{2+x} ($x \leqslant 0.1$) [24], and UO_3 [25]. The shoulder on the high-energy side of the main absorption edge of γ-UO_3 is a multiple-scattering resonance feature characteristic of the axial oxygen atoms from a uranyl (UO_2^{2+}) group [24]. The XANES spectrum of the U-brannerite sample is consistent with the spectrum of the $UO_{2.08}$. Both the edge position as well as the lack of the resonance feature characteristic of the uranyl group indicate that the U-brannerite consists primarily of U(IV) although the presence of U(V) can not be ruled out on the basis of the XANES results.

The EELS data (Fig. 3(a) and (c)) also indicate that Ti and U are predominantly tetravalent in U-brannerite. Fig. 3(a) shows that the main peak positions of Ti in U-brannerite (459.6, 462.8, 465.1, 467.2 eV) compare favorably to those of Ti in the TiO_2 standard (459.7, 461.8, 465.1, 467.2 eV). As noted above, these spectra are quite distinct when compared with the spectrum of trivalent Ti in octahedral coordination (Ti_2O_3).

The O K edge is not in the vicinity of the U $M_{IV,V}$ edge; therefore, the spectra for U are aligned on the U M_{IV} edge. Fig. 3(c) shows that the U peak amplitudes are approximately the same for U-brannerite and the TiO_2. The U M_{IV}/M_V ratios for U-brannerite and the $TiO_2$are both approximately 0.6. For comparison, the U M_{IV}/M_V ratio is close to 0.5 in the hexavalent U standard, $CaUO_4$.

Bright field TEM images revealed the presence of the TiO_2 that was not observed in the BSE images (Fig. 6, top). HRTEM micrographs and SAED indicated that the $U_{0.97}Ti_{2.03}O_{6.00}$ phase was crystalline with no apparent structural defects at the nanoscale (Fig. 6, bottom).

Given the fine-grained nature of the TiO_2 impurity as observed in the bright field TEM image, the EMPA analysis may represent an average composition for the U-brannerite and some TiO_2 particles. However, the stoichiometry calculated from the EMPA results indicated that the brannerite was enriched in Ti by only 1.5 mol%. This will have little effect (<0.5 kJ/mol) on the thermodynamic calculations. Thus, the U-brannerite sample will be treated as a mechanical mixture of 92.5 mol% $U_{0.97}Ti_{2.03}O_{6.00}$, 0.6 mol% UO_2 and 6.9 mol% TiO_2.

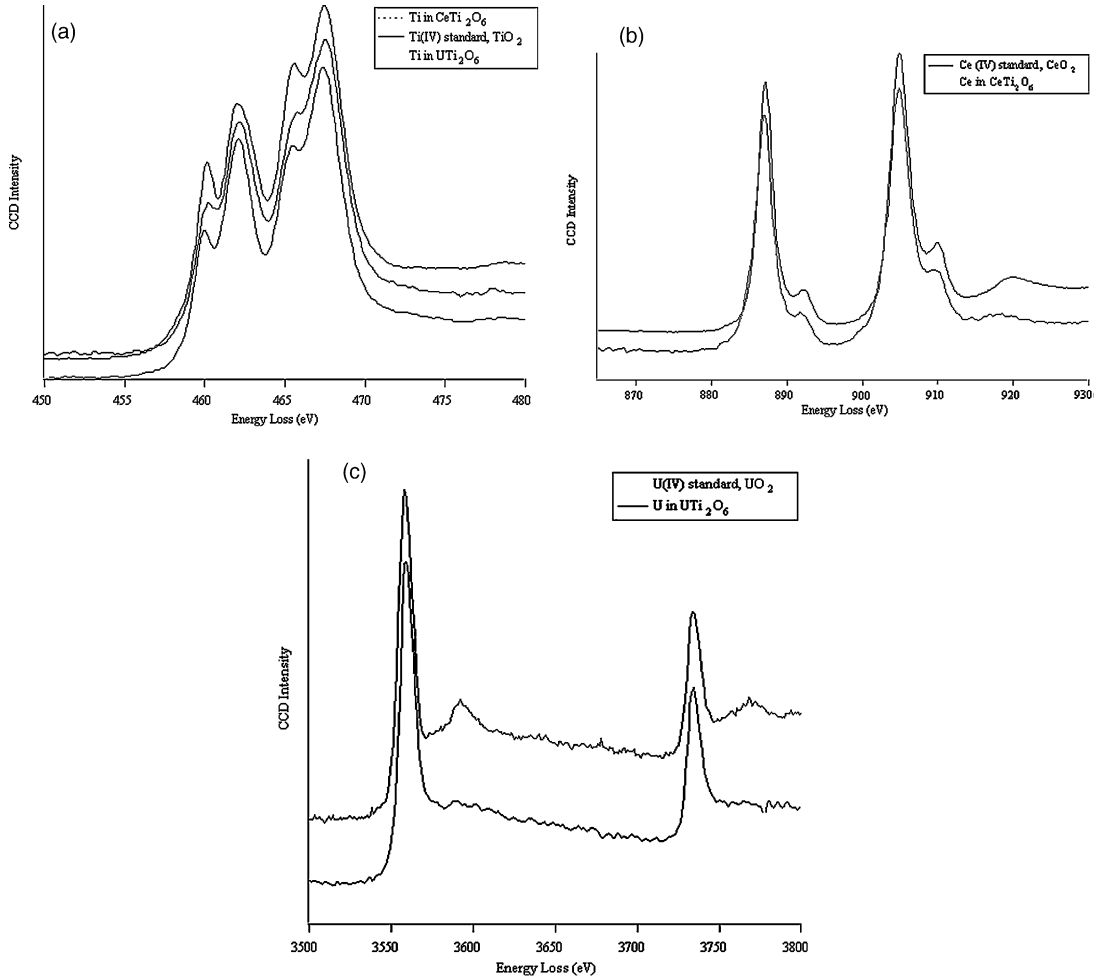

Fig. 3. Electron energy loss spectra for Ti (a), Ce (b) and U (c) in synthetic Ce-brannerite, U-brannerite, TiO_2, CeO_2 and UO_2.

4.3. Th-brannerite: $ThTi_2O_6$

The refined lattice parameters for the Th-brannerite sample are similar to those previously reported for stoichiometric UTi_2O_6 (Table 1) [1]. The Rietveld analysis revealed that the unit cell of $ThTi_2O_6$ is slightly expanded by approximately 0.01 nm (2%) along the *b* and *c* directions relative to UTi_2O_6. This expansion occurs to accommodate the slightly larger Th-ion.

One impurity phase, ThO_2, was identified by XRD. Quantitative phase analysis by the Rietveld method indicated that the Th-brannerite sample consisted of 0.991(3) weight fraction $ThTi_2O_6$ and 0.009(1) weight fraction ThO_2. This converts to 98.7 mol% $ThTi_2O_6$ and 1.5 mol% ThO_2.

The ThO_2 impurity was also observed in BSE images. Semi-quantitative analysis of the digital images indicated that the sample was composed of 0.60 vol.% ThO_2 and 99.40% Th-brannerite. Using the calculated densities of $ThTi_2O_6$ (6.1112 g/cm^3) and ThO_2 (10.0183 g/cm^3) the estimated volume percents were converted to weight percents: 99.02% $ThTi_2O_6$ and 0.98% ThO_2. This is in excellent agreement with the results from powder XRD that indicated the sample consisted of 99.1 wt% $ThTi_2O_6$ and 0.9 wt% ThO_2.

The Th-brannerite sample was analyzed using EMPA-WDS against ThO_2 and TiO_2, rutile, standards. Oxygen was estimated on the basis of stoichiometry (Table 2). The measured Th- and Ti-contents were, within error, equal to the stoichiometric values. The Th-brannerite sample is considered stoichiometric $ThTi_2O_6$ in all subsequent calculations.

TEM bright field imaging indicated that the sample consisted of Th-brannerite (Fig. 7, top). No impurity phases were detected. HRTEM-SAED images revealed extra diffraction spots. These extra spots were attributed to multiple diffraction along the [1 1 0] direction (Fig. 7, bottom). The TEM examination indicated that the

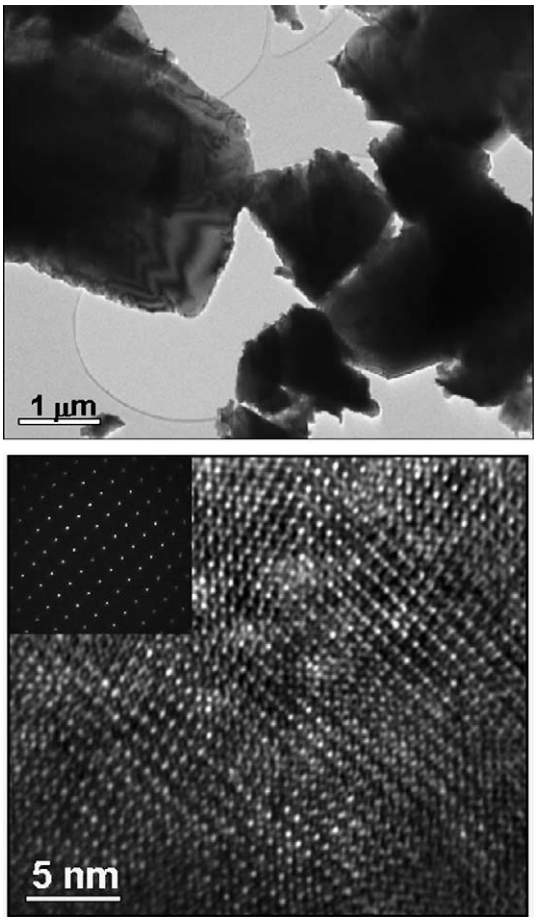

Fig. 4. Bright field image (top), and HRTEM image with SAED pattern (bottom) of Ce-brannerite of the [0 1 0] zone. The sample consists primarily of the Ce-brannerite phase.

sample is crystalline with no apparent structural defects at the nanoscale.

5. Calorimetric methods

High temperature oxide melt solution calorimetry [26,27] was used to measure drop solution enthalpies of the brannerite samples plus their binary oxide components. A Tian–Calvet twin microcalorimeter was used. The details of its design and operation are described in detail elsewhere [26,27]. Prior to calorimetry, the powder samples were dried at 700 °C for a minimum of 1 h. The exceptions to this were the $UO_{2.08}$ and the U-brannerite samples that were dried at 200 °C for 1/2 h to avoid oxidation of the uranium. The solvent used in this study was $3Na_2O \cdot 4MoO_3$, at 975 K. Drop solution enthalpies, ΔH_{ds} were measured by dropping pellets (≈5 mg) of the powdered samples from room temperature into the solvent at calorimeter temperature. Thus, these measurements consist of two components, the heat content of the sample, ${}_{298}\int^{T} C_p \, dT$, and the heat of solution, ΔH_s Solution enthalpies, ΔH_s were measured by equilibrating a pellet above the solvent at calorimeter temperature before dropping the pellet into the solvent. In this manner, the heat content of the sample is eliminated from the signal received by the calorimeter. In both experiments, oxygen was bubbled through the melt to aid in the dissolution of the pellets and to provide high oxygen fugacity that ensured the oxidation of U(IV) to U(VI) [28]. The calorimeters were calibrated using the heat content of α-Al_2O_3 [29]. The measured values of drop solution enthalpies were used in the appropriate thermodynamic cycles to calculate the enthalpies of formation from the oxides. Reference data for the binary oxides were used to calculate the enthalpies of formation from the elements [30].

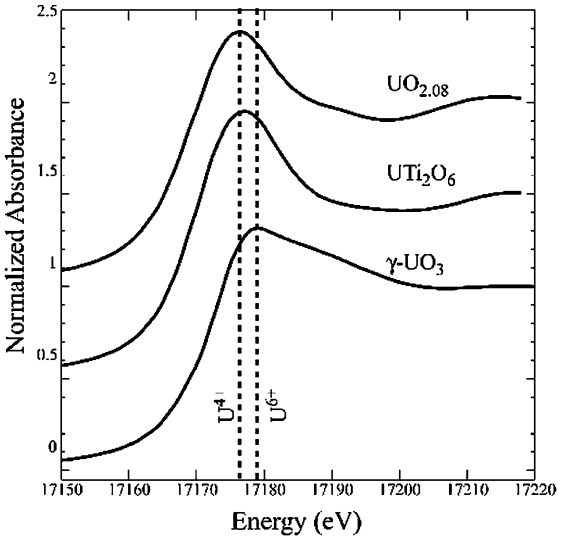

Fig. 5. XANES spectra of $UO_{2.08}$, a U(IV) standard γ-UO_3, a U(VI) standard and U-brannerite. The U L_{III} edge position indicates that the U-brannerite sample consists primarily of U(IV).

6. Calorimetric results

6.1. Enthalpy of formation: Ce-brannerite

Drop solution experiments using $3Na_2O \cdot 4MoO_3$ solvent at 976 K were conducted for CeO_2, TiO_2, rutile and the Ce-brannerite sample (Table 3). The ΔH_{ds} value for the Ce-brannerite sample was corrected for the CeO_2 impurity through a thermodynamic cycle assuming a mechanical mixture of $0.955CeTi_2O_6 + 0.045CeO_2$ (Table 4).

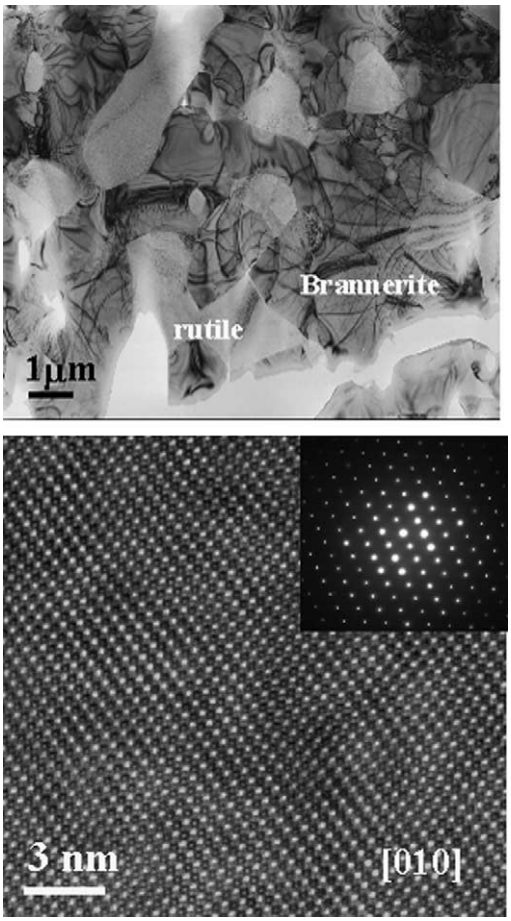

Fig. 6. Bright field TEM image of U-brannerite sample showing two phases U-brannerite and rutile (top). HRTEM micrograph of the [0 1 0] zone of the U-brannerite phase (bottom).

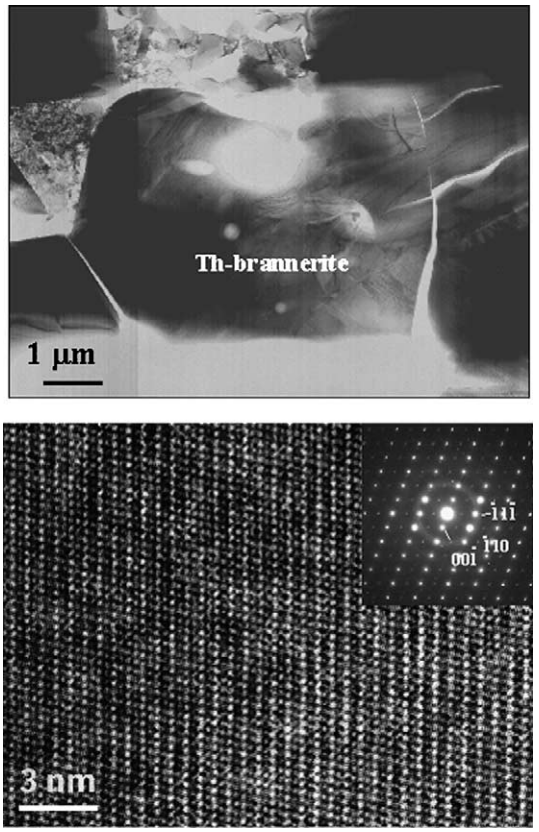

Fig. 7. Bright field image (top), and HRTEM image with SAED pattern (bottom) of Th-brannerite. The sample consists primarily of the Th-brannerite phase. A superstructure appears in the SAED and the HRTEM micrograph.

The ΔH_{ds} value for TiO_2 is consistent with previously published data [31,32]. Prior experiments used the solution calorimetry technique to measure the enthalpy of solution, ΔH_s by equilibrating the TiO_2 above the solvent before mechanically stirring the powder into the solvent. In order to compare the ΔH_{ds} to ΔH_s for TiO_2, the calculated heat content (48.91 kJ/mol) was subtracted from H_{ds} according to the relationship $\Delta H_s = H_{ds} - {}_{298}\int^{976} C_p(TiO_2)\,dT$. The resulting value of 10.02 ± 0.82 kJ/mol falls within the range of previously reported data which ranged from 9.96 to 10.33 kJ/mol [31,32]. The ΔH_{ds} value for CeO_2 in $3Na_2O \cdot 4MoO_3$ solvent at 976 K was previously published and used in a thermodynamic cycle that gave results consistent with observed lanthanide orthophosphate enthalpies [33].

The calorimetric data were used in a thermodynamic cycle to calculate the enthalpy of formation from the oxides, $\Delta H^0_{f\text{-}ox} = +29.4 \pm 3.6$ kJ/mol (Table 4). Using reference data for the standard enthalpies of formation from the binary oxides the standard enthalpy of formation for Ce-brannerite was derived, $\Delta H^0_f = -2948.6 \pm 4.3$ kJ/mol (Table 4).

Table 3
Drop solution enthalpies, ΔH_{ds} and solution enthalpies, ΔH_s used in the thermodynamic cycles

Material	ΔH_{ds} (kJ/mol)	ΔH_s (kJ/mol)
CeO_2	$73.39 \pm 1.65(10)$	
TiO_2	$58.92 \pm 0.82(16)$	
Ce-brannerite	$157.68 \pm 3.04(5)$	
$UO_{2.08}$	$-124.62 \pm 2.30(11)$	
γ-UO_3	$9.49 \pm 1.53(2)$	
U-brannerite	$-1.27 \pm 1.91(7)$	
ThO_2	$0.89 \pm 0.48(3)$	$-47.92 \pm 2.14(3)$
Th-brannerite	$98.01 \pm 1.01(4)$	

Errors are calculated as two standard deviations of the mean. Data was collected using $3Na_2O \cdot 4MoO_3$ solvent at 976 K. Number of experiments is in parentheses.

Table 4
Thermochemical cycles for the calculation of the enthalpies of drop solution, ΔH_{ds} (kJ/mol), for the brannerite samples, correcting for impurities, the enthalpies of formation from the oxides, $\Delta H^0_{f\text{-}ox}$ and the standard enthalpy of formation, ΔH^0_f at 298 K

Reaction		ΔH (kJ/mol)
(1) ΔH_{ds}	Ce-bran (s, 298) $\rightarrow$ [0.955 $CeTi_2O_6$ + 0.045CeO_2] (sln, 976)	157.68 ± 3.04(5)
(2) ΔH_{ds}	CeO_2 (s, 298) $\rightarrow$ CeO_2 (sln, 976)	73.39 ± 1.65(10)
(3) ΔH_{ds}	TiO_2 (s, 298) $\rightarrow$ TiO_2 (sln, 976)	58.92 ± 0.82(16)
(4) ΔH^0_f	Ce (s, 298) + O_2 (g, 298) $\rightarrow$ CeO_2 (s, 298)	−1088.68 ± 1.46[a]
(5) ΔH^0_f	Ti (s, 298) + O_2 (g, 298) $\rightarrow$ TiO_2 (s, 298)	−944.75 ± 1.26[a]
(6) ΔH_{ds}	0.92UO_2 (s, 298) + 0.08UO_3 (s, 298) $\rightarrow$ UO_3 (sln, 976)	−124.62 ± 2.30(11)
(7) ΔH_{ds}	UO_3 (s, 298) $\rightarrow$ UO_3 (sln, 976)	9.49 ± 1.53(2)
(8) $_{298}H^{975}$	1/2 O_2 (g, 298) $\rightarrow$ 1/2 O_2 (g, 976)	9.97[a]
(9) ΔH^0_f	U (s, 298) + O_2 (g, 298) $\rightarrow$ UO_2 (s, 298)	−1084.91 ± 1.00[a]
(10) ΔH^0_f	U (s, 298) + 3/2 O_2 (g, 298) $\rightarrow$ UO_3 (s, 298)	−1223.80 ± 0.80[a]
(11) ΔH_{ds}	U-bran (s, 298) $\rightarrow$ [0.925$U_{0.97}Ti_{2.03}O_6$ + 0.006UO_3 + 0.069TiO_2] (sln, 976)	−1.27 ± 1.91(7)
(12) ΔH^0_f	U (s, 298) + O_2 (g, 298) $\rightarrow$ UO_2 (s, 298)	−1084.91 ± 1.00[a]
(13) ΔH_{ds}	Th-bran (s, 298) $\rightarrow$ [0.987$ThTi_2O_6$ + 0.013ThO_2] (sln, 976)	98.01 ± 1.01(4)
(14) ΔH_{ds}	ThO_2 (s, 298) $\rightarrow$ ThO_2 (sln, 976)	0.89 ± 0.48(3)
(15) ΔH^0_f	Th (s, 298) + O_2 (g, 298) $\rightarrow$ ThO_2 (s, 298)	−1226.41 ± 3.51[a]
Cycle for calculating ΔH_{ds} of $CeTi_2O_6$ correcting for impurities		
(16) ΔH_{ds}	$CeTi_2O_6$ (s, 298) $\rightarrow$ $CeTi_2O_6$ (sln, 976)	
	$[\Delta H(1) - 0.045\,\Delta H(2)]/0.955$	161.65 ± 3.01(5)
Cycle for calculating $\Delta H^0_{f\text{-}ox}$ of $CeTi_2O_6$		
(17) $\Delta H^0_{f\text{-}ox}$	CeO_2 (s, 298) + 2TiO_2 (s, 298) $\rightarrow$ $CeTi_2O_6$ (s, 298)	
	$-\Delta H(16) + \Delta H(2) + 2\,\Delta H(3)$	+29.6 ± 3.6
Cycle for calculating ΔH^0_f of $CeTi_2O_6$		
(18) ΔH^0_f	Ce (s, 298) + 2Ti (s, 298) + 3O_2 (g, 298) $\rightarrow$ $CeTi_2O_6$ (s, 298)	
	$\Delta H(17) + \Delta H(4) + 2\,\Delta H(5)$	−2948.6 ± 4.3
Cycle for calculating ΔH_{ds} of UO_2 correcting for oxidation		
(19) ΔH_{ds}	UO_2 (s, 298) + 1/2 O_2 (g, 976) $\rightarrow$ UO_3 (sln, 976)	
	$[\Delta H(6) - 0.08\,\Delta H(7)]/0.92$	−136.29 ± 2.34
Cycle for calculating $\Delta H^0_{oxidation}$ of UO_2		
(20) $\Delta H^0_{oxidation}$	UO_2 (s, 298) + 1/2 O_2 (g,298) $\rightarrow$ UO_3 (s, 298)	
	Measured $\Delta H(19) - \Delta H(7) + \Delta H(8)$	−135.9 ± 2.8
	Reference $-\Delta H(9) + \Delta H(10)$	−138.8 ± 1.3[a]
Cycle for calculating ΔH_{ds} of $U_{0.97}Ti_{2.03}O_6$ correcting for impurities		
(21) ΔH_{ds}	$U_{0.97}Ti_{2.03}O_6$ (s, 298) $\rightarrow$ 0.97UO_3 (sln, 976) + 2.03TiO_2 (sln, 976)	
	$[\Delta H(11) - 0.006\,\Delta H(19) - 0.069\,\Delta H(3)]/0.925$	−4.87 ± 1.91
Cycle for calculating the $H^0_{f\text{-}ox}$ of $U_{0.97}Ti_{2.03}O_6$		
(22) $\Delta H^0_{f\text{-}ox}$	0.97UO_2 (s, 298) + 2.03TiO_2 (s, 298) $\rightarrow$ $U_{0.97}Ti_{2.03}O_6$ (s, 298)	
	$-\Delta H(21) + 0.97\,\Delta H(19) + 2.03\,\Delta H(3)$	−7.7 ± 2.8
Cycle for calculating the ΔH^0_f of $U_{0.97}Ti_{2.03}O_6$		
(23) ΔH^0_f	0.97U (s, 298) + 2.03Ti (s, 298) + 3O_2 (g, 298) $\rightarrow$ $U_{0.97}Ti_{2.03}O_6$ (s, 298)	
	$\Delta H(22) + 0.97\,\Delta H(12) + 2.03\,\Delta H(5)$	−2977.9 ± 3.5
Cycle for calculating ΔH_{ds} of $ThTi_2O_6$		
(24) ΔH_{ds}	$ThTi_2O_6$ (s, 298) $\rightarrow$ ThO_2 (sln, 976) + 2TiO_2 (sln, 976)	
	$[\Delta H(13) - 0.013\,\Delta H(14)]/0.987$	99.29 ± 1.01
Cycle for calculating $\Delta H^0_{f\text{-}ox}$ of $ThTi_2O_6$		
(25) $\Delta H^0_{f\text{-}ox}$	ThO_2 (s, 298) + 2TiO_2 (s, 298) $\rightarrow$ $ThTi_2O_6$ (s, 298)	
	$-\Delta H(24) + \Delta H(14) + 2\,\Delta H(3)$	+19.4 ± 1.6
Cycle for calculating ΔH^0_f of $ThTi_2O_6$		
(26) ΔH^0_f	Th (s, 298) + 2Ti (s, 298) + 3O_2 (g, 298) $\rightarrow$ $ThTi_2O_6$ (s, 298)	
	$\Delta H(25) + \Delta H(15) + 2\,\Delta H(5)$	−3096.5 ± 4.3

The reaction enthalpies are ΔH_{ds} in $3Na_2O \cdot 4MoO_3$ at 976 K. Number in parentheses is the number of experiments. The error is propagated assuming linear combinations of independent variables.

[a] Data from Ref. [30].

6.2. Enthalpy of formation: U-brannerite

Drop solution experiments were carried out for $UO_{2.08}$, γ-UO_3 and the U-brannerite sample using $3Na_2O \cdot 4MoO_3$ solvent at 976 K (Table 3). The $UO_{2.08}$ sample showed a large exothermic enthalpy of drop solution with $\Delta H_{ds} = -124.62 \pm 2.30$ kJ/mol. The large exothermic ΔH_{ds} along with a color change observed in the solvent from white to yellow indicated that uranium oxidized during dissolution in the melt. The γ-UO_3 generated a small heat signal with less than approximately 0.3 J per experiment. As a result only two of the five experiments had less than five percent relative baseline contributions and were used in further calculations. Usually when the ΔH_{ds} value for a sample is small, the solution calorimetric technique is used. This approach could not be used here because γ-UO_3 is unstable at calorimeter temperature. The ΔH_{ds} value for the U-brannerite sample is approximately zero (-1.27 ± 1.91 kJ/mol). Because the U also would oxidize while this sample was equilibrating at calorimeter temperature, the solution calorimetric technique was not used and we relied on the drop solution data.

The ΔH_{ds} of $UO_{2.08}$ was corrected for the presence of 0.08 mol per formula unit of U(VI) (Table 4). The calculated ΔH_{ds} value for stoichiometric UO_2 is -136.29 ± 2.34 kJ/mol. To cross-check the accuracy of the U drop solution data and to verify that the U(IV) is oxidized to U(VI) in the solvent, reference data for UO_2 and γ-UO_3 were compared to the measured data (Table 4) [28]. The calculated enthalpy of oxidation of UO_2 to γ-UO_3 using measured data was -135.9 ± 2.8 kJ/mol. This is within error equal to the value calculated from reference data, -138.8 ± 1.3 kJ/mol. Therefore, the ΔH_{ds} values for UO_2 and γ-UO_3 are accurate and the final state of uranium in the solvent is U(VI) and is the same whether the starting material contains U(IV) or U(VI).

The ΔH_{ds} value for the U-brannerite sample was corrected for the UO_2 and TiO_2 impurities by assuming a mechanical mixture of 92.5 mol% $U_{0.97}Ti_{2.03}O_{6.00}$, 0.6 mol% UO_2 and 6.9 mol% TiO_2 (Table 4). The enthalpy of formation from the oxides, $\Delta H^0_{f\text{-}ox}$ at 298 K was calculated for the U-brannerite sample (Table 4). The $U_{0.97}Ti_{2.03}O_{6.00}$ is stable with respect to its oxides with $\Delta H^0_{f\text{-}ox} = -7.7 \pm 2.8$ kJ/mol. Reference data were used to calculate the standard enthalpy of formation from the elements, $\Delta H^0_f = -2977.9 \pm 3.5$ kJ/mol (Table 4).

There are two potential sources of error in the calculation of ΔH^0_f of U-brannerite. One is that the presence of a small amount of U(V) can not be eliminated on the basis of the XANES analysis. The smaller U(V) (ionic radius = 0.076 nm, CN = 6) would facilitate the apparent cation mixing observed in U-brannerite and result in a decrease in the lattice parameters that were attributed to the sub-stoichiometric U in the sample [12]. However, no reports of U(V) in brannerite in the absence of aliovalent dopant cations such as Ca or Gd have been reported in the literature. Therefore, the presence of pentavalent uranium in this sample is unlikely. The second potential source for error is in the EMPA-WDS results. Any slight oxidation of the U metal standard used in the analysis would cause an underestimation of the U-content in the sample. In order to assess this uncertainty, the $\Delta H^0_{f\text{-}ox}$ was calculated for the calorimetric data assuming the U-brannerite was stoichiometric UTi_2O_6. This value -13.6 ± 2.9 kJ/mol, is approximately 6 kJ/mol more exothermic than that calculated for the U-deficient brannerite. The $\Delta H^0_{f\text{-}ox} = -7.7 \pm 2.8$ kJ/mol calculated for the non-stoichiometric U-brannerite is more conservative (in terms of assessing stability) and was used in all subsequent thermodynamic calculations in this study.

6.3. Enthalpy of formation: Th-brannerite

Drop solution experiments were conducted for ThO_2 and the Th-brannerite sample using $3Na_2O \cdot 4MoO_3$ solvent at 976 K (Table 3). The ThO_2 gave a small thermal signal (<0.15 J per experiment). As a result these data were checked by conducting solution calorimetry where the ThO_2 sample was equilibrated at calorimeter temperature before lowering into the solvent for dissolution. The ΔH_{ds} less the heat content of the sample should equal the enthalpy of solution: $\Delta H_{ds} - {}_{298}\int^{976} C_p \, dT = \Delta H_s$ The measured heat content of ThO_2 was 50.13 ± 0.51 kJ/mol [34]. This is, within error, equal to the tabulated heat content value of 50.5 kJ/mol [28]. The calculated enthalpy of solution is $\Delta H_s = -49.24 \pm 0.70$ kJ/mol. This value compares well with the measured heat of solution for ThO_2, $\Delta H_s = -47.94 \pm 2.14$ kJ/mol. Thus, the measured value for the ΔH_{ds} for ThO_2 (0.89 ± 0.48 kJ/mol), although small, is accurate and was used in all subsequent thermodynamic calculations.

The ΔH_{ds} value for Th-brannerite was corrected for the small amount of ThO_2 impurity (Table 4). The enthalpy of formation from the oxides, $\Delta H^0_{f\text{-}ox}$ at 298 K for $ThTi_2O_6$ was calculated (Table 4). Th-brannerite is metastable with respect to its oxides with $\Delta H^0_{f\text{-}ox} = +19.4 \pm 1.6$ kJ/mol. Reference data were used to calculate the standard enthalpy of formation from the elements, $\Delta H^0_f = -3096.5 \pm 4.3$ kJ/mol (Table 4).

7. Discussion

7.1. The role of entropy in the stabilization of brannerite

Both $CeTi_2O_6$ and $ThTi_2O_6$ have positive enthalpies of formation from the oxides with $\Delta H^0_{f\text{-}ox}$ equal to $+29.4 \pm 3.6$ and $+19.4 \pm 1.6$ kJ/mol respectively. A positive $\Delta H^0_{f\text{-}ox}$ generally indicates that the compound has

limited stability or is metastable. Stability is determined by the value of the free energy, ΔG^0_{rxn} for a given reaction according to the relationship:

$$\Delta G^0_{rxn} = \Delta H^0_{rxn} - T(\Delta S^0_{rxn}). \quad (1)$$

For compounds with positive ΔH^0_{rxn} to have negative ΔG^0_{rxn} the $-T(\Delta S^0_{rxn})$ term must be sufficient to offset the enthalpy. As T increases so does the impact of the $-T(\Delta S^0_{rxn})$ term. Therefore, entropy stabilized compounds may be unstable with respect to decomposition to their binary oxides below some critical temperature, though often slow kinetics may hinder decomposition. Many examples of entropy stabilized compounds have been reported, e.g., mullite and pseudobrookite [35].

In order to estimate the entropy contribution for the reaction $MO_2 + 2TiO_2 \rightarrow MTi_2O_6$ where M = Ce and Th, Eq. (1) was solved for $\Delta G^0_{f\text{-}ox} \leqslant 0$ where T was given by the synthesis temperature. The $CeTi_2O_6$ sample was synthesized at 1623 K. The lower limit for $\Delta S^0_{f\text{-}ox}$ is, therefore, given by:

$$0 \geqslant \Delta G^0_{f\text{-}ox} = H^0_{f\text{-}ox} - T(\Delta S^0_{f\text{-}ox}), \quad (2)$$

$$\Delta S^0_{f\text{-}ox} \geqslant \Delta H^0_{f\text{-}ox}/T = (29\,380 \pm 3630\ \mathrm{J/mol})/1623\ \mathrm{K} = 18.1 \pm 2.2\ \mathrm{J\,K^{-1}\,mol^{-1}}. \quad (3)$$

The $ThTi_2O_6$ sample was synthesized at 1723 K. The lower limit for $\Delta S^0_{f\text{-}ox}$ is, therefore, given by:

$$\Delta S^0_{f\text{-}ox} \geqslant \Delta H^0_{f\text{-}ox}/T = (19\,440 \pm 1610\ \mathrm{J/mol})/1723\ \mathrm{K} = 11.3 \pm 1.0\ \mathrm{J\,K^{-1}\,mol^{-1}}. \quad (4)$$

These are probably underestimates because the compounds are almost certainly thermodynamically stable somewhat below their synthesis temperature.

Configurational entropy likely contributes significantly to the stability of brannerite. The non-stoichiometry commonly observed in U-bearing brannerite indicates that a small, but significant mixing of Ti may occur on the U-site. This cation mixing may also occur in other brannerite compositions. In order to investigate this hypothesis, a detailed structural investigation of the crystallographic site occupancies would be required.

7.2. Trends in the enthalpy of formation of brannerite and the prediction of $PuTi_2O_6$ energetics

A plot of the ionic radius of the M-site cation (CN = 6, M^{4+}) versus the enthalpy of formation from the oxides, $\Delta H^0_{f\text{-}ox}$, for the three brannerite phases defines a non-linear trend (Fig. 8), with a clear minimum near the ionic radius of uranium [10]. Both the Ce- and Th-bearing brannerite samples are stoichiometric and energetically metastable with respect to their binary oxides. The U-brannerite is non-stoichiometric and energetically stable with respect to its binary oxides.

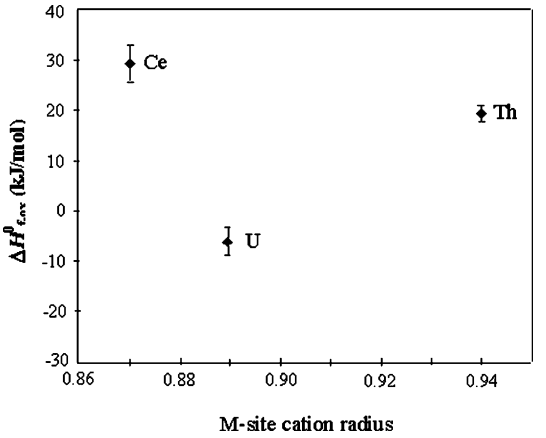

Fig. 8. The enthalpy of formation from the oxides, $\Delta H^0_{f\text{-}ox}$ of three brannerite phases versus the M-site ionic radius (CN = 6, M^{4+}) [10]. Both the Ce- and Th-brannerite samples are metastable with respect to their oxide assemblages. U-brannerite is stable with respect to its oxides.

A phenomenological explanation for this trend may be inferred from the XRD data. In both the Ce- and Th-brannerite samples the refined lattice parameters deviate slightly, but significantly from those reported for U-brannerite (see Table 1). The Ce-brannerite sample, relative to the U-brannerite, is expanded along the *a*-axis, and shortened along the *b* and *c* axes. The net result is a shortening of the distance between the anatase-type sheets concurrent with additional distortions within these layers. The Th-brannerite sample has a 2% expansion in both the *b* and *c* directions. The net result is a lengthening of the distance between the anatase-type layers. These results are consistent with the varying ionic radii from the smaller Ce ion (0.087 nm, CN = 6) to the larger Th ion (0.094 nm, CN = 6) [10]. The thermochemical data suggest that there is an ideal (i.e., most stable) separation distance between the anatase-type layers that is approached when U is the predominant cation on the M-site.

An analogous trend was observed in ion beam irradiation studies of these same three brannerite samples [8,9]. The 'relative' resistance of each brannerite composition to radiation-induced amorphization can be assessed by comparing their critical amorphization doses, D_c, at room temperature [8,9]. Using the U-brannerite as a baseline, D_c at room temperature increased in this order: $D_c(CeTi_2O_6) < D_c(ThTi_2O_6) < D_c(UTi_2O_6)$ [8,9]. This is the same trend observed for the enthalpy measurements. $CeTi_2O_6$ is the least stable with respect to its oxides and the most easily amorphized of the three compositions. UTi_2O_6 is the most stable in enthalpy and is most 'resistant' to radiation damage. The resistance of a phase to radiation damage is related to its thermodynamic stability and the ability to epitaxially anneal the damage along the boundaries of the cascade [36].

Previous work reported that the synthesis of $PuTi_2O_6$ was extremely difficult [11]. Significant (>70 wt%) yields were achieved only with sintering at approximately 95% of the melting temperature, 1550 °C. Even then a maximum yield of only 75 wt% brannerite was achieved [11]. The impurity phases in all syntheses were the binary oxides, PuO_2 and TiO_2. This suggests that $PuTi_2O_6$ has a limited temperature range of stability and a small thermodynamic driving force for its formation. An estimate of the formation enthalpy of $PuTi_2O_6$ was made by assuming that $\Delta S^0_{\text{f-ox}}(CeTi_2O_6) \approx \Delta S^0_{\text{f-ox}}(PuTi_2O_6) = 18 \pm 4.4\ \text{J K}^{-1}\,\text{mol}^{-1}$. The uncertainty is estimated as twice the uncertainty of the Ce value. Then setting $\Delta G^0_{\text{f-ox}} = 0$ at the synthesis temperature of 1823 K, $\Delta H^0_{\text{f-ox}}$ is 33 ± 8 kJ/mol. This reasoning and the data for $CeTi_2O_6$ suggest that $PuTi_2O_6$ will be significantly energetically metastable with respect to its binary oxides, and metastable in terms of free energy at all but very high (>1500 °C) temperature, an observation consistent with the synthesis difficulties.

7.3. The impact of brannerite on waste form stability

The phase assemblages in the proposed titanate waste form for plutonium immobilization can be described by a pseudoquaternary phase diagram. The nominal compositions for the end-member phases are: Hf-zirconolite or 'hafnolite', $CaHfTi_2O_7$; Gd-titanate pyrochlore, $Gd_2Ti_2O_7$; U-pyrochlore, $CaUTi_2O_7$ and Pu-pyrochlore, $CaPuTi_2O_7$ [6]. The baseline waste form ceramic consists of (wt%) CaO – 10.0; HfO_2 – 10.6; TiO_2 – 35.9; Gd_2O_3 – 7.9; UO_2 – 23.7 and PuO_2 – 11.9. The total actinide-oxide fraction is nearly 36 wt%. Such a high actinide content requires the presence of neutron absorbers to lessen the possibility of criticality. Hence gadolinium oxide and hafnium oxide are present in the baseline composition.

The final ceramic product contains the following average phase proportions (vol.%): pyrochlore – 80, brannerite – 12, zirconolite – 0, rutile – 8 and actinide oxide – 0.5 [6]. The major actinide-bearing impurity observed was brannerite, MTi_2O_6, where M = actinide. If actinides were absent during synthesis, brannerite did not form. A mixture of CeO_2 and TiO_2 formed instead. Adding UO_2 to the initial mixture increased the pyrochlore yield (≈80 vol.%) with brannerite, UTi_2O_6, being the major impurity (≈12 vol.%) plus minor amounts of TiO_2 (≈8 vol.%) and a U-Ca oxide compound (<1 vol.%) [6]. The observed range for brannerite content was from 0 to 22 vol.% (⩽30 wt%).

A recent assessment of the thermodynamic stability of the titanate waste form based on a consideration of the pyrochlore and zirconolite end-member Gibbs energies of formation has recently been made [37]. This study concluded that the proposed waste form composition is stable with respect to both an oxide assemblage and an oxide plus perovskite assemblage [37]. This assessment assumed ideal mixing of the pyrochlore/zirconolite end-members and did not account for intermediate compound formation or the presence of impurity phases such as brannerite.

A summary of the enthalpies of formation of the relevant waste form components is given in Table 5. The three pyrochlore end-members are all stable with respect to their binary oxides. The U-pyrochlore is marginally stable with respect to a perovskite plus oxide assemblage. The Ce-pyrochlore is metastable with respect to perovskite plus oxides. Assuming ideal mixing, the enthalpy of formation at 298 K from the perovskite plus oxide assemblage, $\Delta H_{\text{f-pv+ox}}$ for the baseline waste form ceramic is calculated as a weighted average of the end-member contributions (mol frxn) [37]:

$$0.24(CaHfTi_2O_7) + 0.10(Gd_2Ti_2O_7) + 0.42(CaUTi_2O_7) + 0.23(CaPuTi_2O_7), \quad (5)$$

$0.24(+6.0 \pm 3.5) + 0.10(-113.4 \pm 2.8) + 0.42(-5.1 \pm 4.0) + 0.23(+21.0 \pm 6.0) = -7.6 \pm 4.3$ kJ/mol.

The brannerite compositions that formed during syntheses of the waste form ceramic all contained a mixture of U and Pu with minor amounts of Hf, Gd and

Table 5
A summary of the thermodynamic data for the components of the waste form for excess weapons plutonium

Material	$\Delta S^0_{\text{f-ox}}$ (J/mol K)	$\Delta H^0_{\text{f-ox}}$ (kJ/mol)	ΔH^0_{f} (kJ/mol)
Ce-pyrochlore	16.4 ± 0.5[a]	-54.2 ± 5.2[a]	-3656.0 ± 5.6[a]
U-pyrochlore	20.9 ± 0.3[a]	-123.7 ± 3.4[a]	-3610.6 ± 4.1[a]
Gd-pyrochlore	–	-113.4 ± 2.8[a]	-3822.5 ± 4.9[a]
Ce-brannerite	18.1 ± 2.2	$+29.4 \pm 3.6$	-2948.8 ± 4.3
U-brannerite	–	-7.7 ± 2.8	-2977.9 ± 3.5
Th-brannerite	11.3 ± 1.0	$+19.4 \pm 1.6$	-3096.5 ± 4.3
Pu-brannerite	–	$+33 \pm 8$	-2909 ± 8

The entropy values for the brannerite phases were estimated assuming $\Delta G^0_{\text{f}} \leqslant 0$ at synthesis temperatures.

[a] Data taken from Ref. [37] actual pyrochlore compositions: Ce-pyrochlore $Ca_{0.93}CeTi_{2.04}O_7$; U-pyrochlore $Ca_{1.46}U^{4+}_{0.23}U^{6+}_{0.46}Ti_{1.85}O_7$; Gd-pyrochlore $Gd_2Ti_2O_7$.

Ca on the M-site and were U-rich with approximately four times as much U+impurity cations as Pu [6,7]. Using an average brannerite composition of $U_{0.8}Pu_{0.2}Ti_2O_6$, and assuming U replaces the impurity cations, we can estimate an enthalpy of formation from the oxides. Assuming that ideal mixing occurs between the U- and Pu-brannerite end-members, the $\Delta H^0_{\text{f-ox}}$ is given by a weighted average of the end-member enthalpies:

$$0.8\,\Delta H^0_{\text{f-ox}}(\text{U-brannerite}) + 0.2\,\Delta H^0_{\text{f-ox}}(\text{Pu-brannerite}) = \Delta H^0_{\text{f-ox}}(U_{0.8}Pu_{0.2}Ti_2O_6). \quad (6)$$

Thus, the $\Delta H^0_{\text{f-ox}}(U_{0.8}Pu_{0.2}Ti_2O_6) \approx +0.4 \pm 3.4$ kJ/mol. This suggests that despite the significant metastability of the Pu- and Th-brannerite end-members, the brannerite in the waste form may be only marginally energetically metastable in enthalpy with respect to decomposition to its binary oxides. Two factors contribute to brannerite stability in the waste form ceramic, a high U-content and significant cation mixing on the M-site (not accounted for in this estimation). Assuming an ideal mixture of 30 wt% (32.5 mol%) brannerite and 70 wt% (67.5 mol%) baseline waste form ceramic, the overall enthalpy of formation at 298 K can be estimated:

$$\begin{aligned} &0.325\,\Delta H_{\text{f-ox}}(U_{0.8}Pu_{0.2}Ti_2O_6) \\ &\quad + 0.675\,\Delta H_{\text{f-pv+ox}}(\text{baseline ceramic}) \\ &\quad = 0.325(+0.4 \pm 3.4) + 0.675(-7.6 \pm 4.3) \\ &\quad = -5.0 \pm 4.8\text{kJ/mol}. \end{aligned} \quad (7)$$

The presence of up to 30 wt% brannerite in the ceramic will, therefore, not significantly decrease the thermodynamic stability of the waste form.

8. Conclusions

Ce- and Th-brannerite are higher in energy than their binary oxides with $\Delta H^0_{\text{f-ox}} = (+29.4 \pm 3.6)$ and $(+19.4 \pm 1.6)$ kJ/mol respectively. These materials are entropy stabilized with $\Delta S^0_{\text{f-ox}}(CeTi_2O_6) = 18.1 \pm 2.2$ and $\Delta S^0_{\text{f-ox}}(ThTi_2O_6) = 11.3 \pm 1.0$ $\text{J mol}^{-1}\,\text{K}^{-1}$. U-brannerite is energetically stable with respect to its binary oxides by -7.7 ± 2.8 kJ/mol. This is consistent with the relative ease of formation of this material. The trend in the enthalpies of formation is the same trend observed for the critical amorphization doses, D_c, at room temperature for the three compositions. $CeTi_2O_6$ is the least stable with respect to its oxides and the most easily amorphized. UTi_2O_6 is the most stable in enthalpy and is the most 'resistant' to radiation damage. The $\Delta H^0_{\text{f-ox}}$ for $CeTi_2O_6$ provides an adequate estimate the $\Delta H^0_{\text{f-ox}}$ for $PuTi_2O_6 \approx +33$ kJ/mol. Despite significant metastability of the end-member Pu- and Th-brannerite compositions at low temperature, the presence of large amounts (up to 30 wt%) of brannerite in the final ceramic is not likely to significantly decrease waste form stability.

Acknowledgements

Financial support was provided by Lawrence Livermore National Laboratory, the Department of Energy EMSP grant number 60118 at Livermore and grant number DE-FG07-97ER45673, the University of California at Davis and by the Office of Basic Energy Sciences, DOE grant DE-FG02-97ER45656 (to R.C. Ewing at the University of Michigan). Portions of this research were carried out at the Stanford Synchrotron Radiation Laboratory, a national user facility operated by Stanford University on behalf of the US Department of Energy, Office of Basic Energy Sciences. G.R.L. and M.C. thank Mark Blackford for maintaining the JEOL 2010F/GIF to a high operational level and Kath Smith for guidance in the interpretation of EELS data.

References

[1] J.T. Szymanski, J.D. Scott, Can. Mineral. 20 (1982) 271.
[2] W.I. Finch, US Geol. Surv. Bull. 2141 (1996) 18.
[3] R.J. Finch, T. Murakami, in: P.C. Burns, R. Finch (Eds.), Uranium: Mineralogy, Geochemistry and the Environment, Reviews in Mineralogy, vol. 38, 1999, p. 91.
[4] A.E. Ringwood, S.E. Kesson, K.D. Reeve, D.M. Levins, E.J. Ramm, in: W. Lutze, R.C. Ewing (Eds.), Radioactive Waste Forms for the Future, 1988, p. 233.
[5] A. Jostsons, L. Vance, B. Ebbinghaus, in: Proceedings of the International Conference on Future Nuclear Systems, Global 99, Jackson Hole, Wyoming, American Nuclear Society CDROM, 1999.
[6] B.B. Ebbinghaus, R.A. von Konynenburg, E.R. Vance, A. Jostsons, R.G. Anthony, D.J. Wronkiewicz, in: Proceedings of the Department of Energy Plutonium Stabilization and Immobilization Workshop, 1995, p. 253.
[7] S.I. Martin, O.H. Krikorian, B.B. Ebbinghaus, E.R. Vance, R. Putnam, Synthesis and Characterization of Cerium Titanate and Related Titanate Phases in the Development of a Ceramic Immobilization Form, LLNL Internal Report, 1999.
[8] G.R. Lumpkin, K.L. Smith, M.G. Blackford, J. Nucl. Mater. 289 (2001) 177.
[9] J. Lian, L.M. Wang, G.R. Lumpkin, R.C. Ewing, Nucl. Instrum. and Meth. Phys. B 191 (1–4) (May 2002) 565.
[10] R.D. Shannon, Acta Cryst. A 32 (1976) 751.
[11] E.R. Vance, J.N. Watson, M.L. Carter, R.A. Day, B.D. Begg, J. Am. Ceram. Soc. 84 (1) (2001) 141.
[12] M.W.A. Stewart, E.R. Vance, R.A. Day, Report on Phase 2 of Task 1.1: Single phase synthesis, LLNL # B345772, 1999.
[13] F.D. Bloss, Crystallography and Crystal Chemistry, 2nd Ed., Mineralogical Society of America, Washington, DC, 1994, p. 545.

[14] P.C. Burns, in: P.C. Burns, R. Finch (Eds.), Uranium: Mineralogy, Geochemistry and the Environment, Reviews in Mineralogy, vol. 38, 1999, p. 23.
[15] C. Frondel, US Geol. Surv. Bull. 1064 (1958) 400.
[16] K.D.P. Singh, L.R. Bhargava, M.A. Ali, B.M. Swarnkar, Explor. Res. At. Miner. [India] 1 (1990) 117.
[17] G.R. Lumpkin, R.C. Ewing, Am. Mineral. 81 (1996) 1237.
[18] C. Miyake, D. Sugiyama, M. Mizuno, J. Alloys Compd. 213&214 (1994) 516.
[19] A.C. Larson, R.B. von Dreele, GSAS. General Structure Analysis System, LANSCE, MS-H805, Los Alamos, New Mexico, 1994.
[20] W.J. Weber, R.C. Ewing, et al. (including Alex), J. Mater. Res. 13 (1998) 1434.
[21] R.C. Ewing, W.J. Weber, F.W. Clinard Jr., in: Progress in Nuclear Energy, vol. 29, 1995, p. 63.
[22] RIQAS software from Materials Data, Inc.
[23] G.N. George, I.F. Pickering, Stanford Synchrotron Radiation Laboratory, Stanford, CA, 1995. Available from <http://ssrl.slac.stanford.edu/exafspak.html>.
[24] F. Farges, C.W. Ponader, G. Calas, G.E. Brown, Geochim. Cosmochim. Acta 56 (1992) 4205.
[25] P.M. Bertsch, D.B. Hunter, S.R. Sutton, S. Bajt, M.L. Rivers, Environ. Sci. Technol. 28 (5) (1994) 980.
[26] A. Navrotsky, Phys. Chem. Miner. 2 (1977) 89.
[27] A. Navrotsky, Phys. Chem. Miner. 24 (1997) 22.
[28] A. Navrotsky, J. Therm. Anal. Calorim. 57 (1999) 653.
[29] NBS certificate: standard reference material 720, April, 1982.
[30] R.A. Robie, B.S. Hemingway, US Geol. Surv. Bull. 2131 (1995).
[31] A. Navrotsky, O.J. Kleppa, J. Am. Ceram. Soc. 50 (1967) 626.
[32] A. Navrotsky, O.J. Kleppa, J. Inorg. Nucl. Chem. 30 (1968) 479.
[33] S.V. Ushakov, K.B. Helean, A. Navrotsky, L.A. Boatner, J. Mater. Res. 16 (9) (2001) 2623.
[34] R.L. Putnam, PhD dissertation, Princeton University, 1999.
[35] A. Navrotsky, Am. Mineral. 79 (1994) 589.
[36] S.X. Wang, L.M. Wang, R.C. Ewing, Phys. Rev. B 63 (2001) 024105.
[37] K.B. Helean, A. Navrotsky, E.R. Vance, M.L. Carter, B. Ebbinghaus, O. Krikorian, J. Lian, L.M. Wang, J.G. Catalano, J. Nucl. Mater. 303 (2002) 226.